Experimental Study on the Pitting Detection Capabilities for Spur Gears Using Acoustic Emission and Vibration Analysis Methods

M. Grzeszkowski, C. Gühmann, P. Scholzen, C. Löpenhaus, S. Nowoisky and G. Kappmeyer

Introduction

To run all components of an aero engine at optimal speeds a planetary gearbox between fan and turbine is required. This new aero engine design allows slow fan rotation together with high turbine speed. As a result, the efficiency and bypass ratio increase significantly. However, using a gearbox introduces additional failure modes such as gear wear, pitting and gear teeth cracks.

Usually, high attention is paid to pitting initiation since this failure mode leads to subsequent destructive failures. Therefore, the early detection of pitting using a feature-based condition monitoring system is recommended to avoid unplanned engine shutdown and expensive gear replacements.

This paper describes an experimental investigation on spur gears to characterize the pitting degradation process using monitoring features.

Specific question or relationship. Previous investigations have revealed that pitting has an impact on the gear vibration behavior (Ref. 27). But is it possible to detect pitting at an early stage using acceleration sensors and acoustic emission (AE) sensors to avoid consequential damages and subsequent correction activities?

It is assumed that the pitting initiation process begins with the excitation of high frequency AE impulses above 50 kHz. Moreover, pitting progression causes increased sidebands in the gear mesh order spectrum. Therefore, the AE sensor technique with a higher bandwidth seems to be more suitable for early pitting detection.

The main goal of this experimental investigation is to understand, if an early pitting detection can be achieved using AE sensors combined with appropriate signal processing methods.

Method. The authors investigated several gears manufactured with different pitch deviations and surface properties. The gears were pre-loaded in a back-to-back test rig and driven until distinctive pitting occurred. Multiple acceleration sensors and AE sensors are mounted on the stationary housing adjacent to the gear bearing shell.

The sensors measure the vibration characteristics of the intermeshing gears. The signals were then filtered, resampled and pattern recognition methods were applied to extract monitoring features (Ref. 4). These features allowed a conclusion to be made regarding the correlations between those features and the pitting degradation process of the gears.

Results. For pitting detection, the AE sensors seem to be more suitable due to their higher bandwidth in comparison to the industrial acceleration sensors, for which the bandwidth ends around 50 kHz. The results show that a detection of pitting is possible several hours before complete gear failure. The test run results also depict the advantages and disadvantages of both the acceleration and the AE sensors.

Conclusion. The results indicate that early detection of pitting damage is possible. Based on the results, the requirements for potential production sensors and the corresponding signal processing algorithms can be defined for the integration in the control monitoring system for future aero engines. Furthermore, the influence of manufacturing processes and manufacturing deviations on the pitting progression can be investigated. A correlation between different finish qualities and the last machining step must be assessed to identify the associated impact on surface integrity.

The following introduces the requirements to monitor a planetary gearbox integrated in future aero engines followed by the fundamentals regarding the pitting. Afterwards the generation of acoustic emission due to pitting development will be presented and how the pitting affects the gear vibration behavior.

Power Gearbox Monitoring

Engine manufacturers are developing a power gearbox capable to transfer up to 100,000 horsepower. The technology will be demonstrated to achieve those levels. The trend of increasing flight capacities for the next decades indicates a strong demand of efficient propulsion systems. Further aspect is the demand to reduce the noise of power plants. To reduce the noise and make the power plant more efficient a power gearbox must be introduced between fan-shaft and turbomachinery. The planetary gearbox allows the Fan to rotate slower than the fast-rotating core engine. The associated improvement in efficiency and reduction in weight will allow the UltraFan to offer a 25% fuel efficiency improvement over the first generation of engines (Ref. 1). It is common state-of-the-art to monitor high-value machines during operation. The power gearbox is a new technology. The capability to monitor such a power gearbox will be increased in parallel to the hardware development. The requirements to monitor the power gearbox are made evident by the use of various system design tools, e.g. — *Functional Failure Mode* and *Effect Analysis* (FFMEA).

The assessments depict a clear demand to monitor the geartrain to depict typical gear failures such as gear wear, pitting and gear teeth cracks (Ref. 2). Depending on the failure progression, different effects, e.g. — acoustic emission (AE), vibration, particles or heat — could be measured to indicate an impending failure (Ref. 3). An important requirement is the early failure indication and the subsequent correction activity without disrupting the operation of the customers.

Former research (Ref. 4) worked to identify viable methods to detect geartrain failures based on subscale test environments. The next step is to use subscale component test rigs with comparable gear material, geometry and gear quality. This paper answers the question: what kind of sensor fits for the purpose of early geartrain failure indication? To prove theoretical ideas, subscale component rigs are more efficient than full-scale application. To improve the geartrain monitoring capability ahead of the used back-to-back (B2B) configuration presented in this paper, further experiments are planned. The next test vehicles are based on subscale and full-scale power gearbox applications.

Pitting Damage and Phenomenological Models

The main fatigue damage that occurs in the tooth flank area is not only micropitting and flank fracture, but also macropitting damage. If the local rolling strength of the edge zone is exceeded, pitting damage occurs, which is characterized by a shell-shaped triangular breakout (Ref. 5). The breakout surface propagates parallel to the tooth flank surface. With respect to the tooth flank, pitting damage preferably occurs below the pitch diameter in the area of negative slippage. The tip of the triangle shape points in the direction of the tooth root, and thus in the same direction as the tangential or frictional force related to the damaged surface (Ref. 6). Different phenomenological models exist for the development of pitting damage, which differentiate between surface and sub-surface-induced pitting damage (Fig. 1; Ref. 7).

Surface-induced pitting damage is caused by surface material cracks due to periodically rolling stress (Refs. 5 and 8). The breakout of particles can be explained by the fusion of individual cracks or the hydraulic blasting effect of the lubricant (Refs. 6 and 9). The characteristic fluid incompressibility of the oil leads to an increase in stress in the notch of the crack gap during over rolling, since the rolling movement closes the crack in the area of the negative slip and the oil cannot escape. In contrast, sub-surface-induced tooth flank damage occurs due to crack initiation below the surface. According to Ding, the crack initiation takes place at material defects in the surface zone (Ref. 10). Further crack propagation is supported by the cyclic alternating stress in the surrounding area of the initial crack. The connection to the fatigued zone, which starts at the crack end of the initial crack, leads to an enlargement of the total crack. The high pressure and shear stresses in the intermediate areas lead to the failure of the undercut particles, and thus to deep pitting damages (Refs. 10–11). On one hand, global analytical phenomenological approaches provide the calculation of the standard load-bearing capacity, according to ISO 6336 or AGMA 2001 (Refs. 12–13). On the other hand, local numerical material physical calculation methods based on the concept of local fatigue strength were developed (Refs. 14–15). In all methods, the present stress state is compared by forming a reference stress with a permissible stress of the material (Ref. 16).

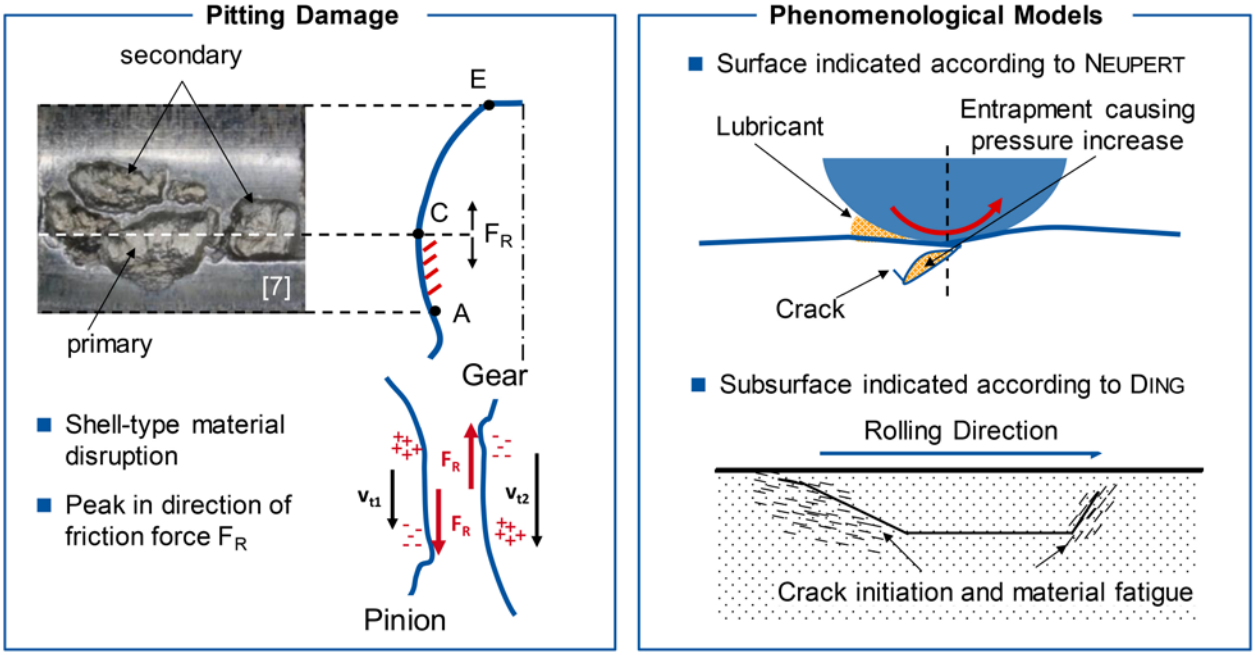

Figure 1 Pitting damage and phenomenological models (Refs. 7, 11 and 27).

Experimental Investigations on Pitting Detection

Due to the fact that pitting is caused primarily through crack initiation below the tooth surface and in the surface area, these material defects lead to a disturbed vibration characteristic during periodic load of the spur gears. Cracks at the tooth surface zone result in an excitation of elastic waves within the material, which lead to AE signals (Ref. 17; Fig. 2). This distinctive crack damage leads to particle breakout that directly influences the mesh stiffness of the teeth. Depending on the distribution of those particle breakouts, an additional vibration excitation of the gears can be observed in the vibration spectrum (Ref. 17). With the foregoing considerations there are two principle sensor methods, which potentially allow a pitting detection, i.e. — acceleration sensors and AE sensors.

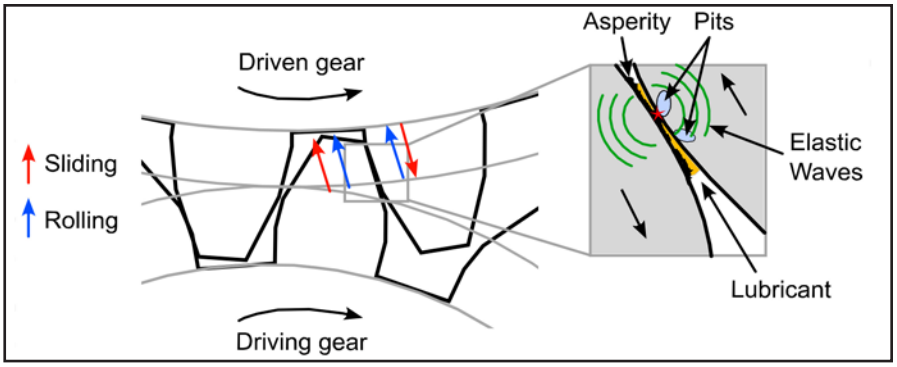

Figure 2 Initiation of elastic waves during negative sliding contact (Ref. 18).

The following authors already studied the possibility of detecting the pitting progression during operation conditions using vibration and other type sensors. Cheng (Ref. 18) used dynamic models for healthy and pitted gears to carry out sensitive and robust features, and to calibrate and normalize them. Pitting was artificially induced and the accelerometer signals were acquired to estimate the pitting severity of the gearset. Tan (Ref. 20) compared accelerometer measurements, AE measurements and spectrometric oil analysis to their capability of detecting naturally caused pitting. Their results showed a high sensitivity of AE RMS value to sliding speed on the tooth flank and tooth stresses. Additionally, an increased AE amplitude with increasing pitting breakout zone could be observed. Tan also concluded that the AE measurement method is suitable for early pitting detection. There are also publications where the authors investigated the causes of macro- and micropitting initiation using other equipment, such as microscopes, CNC gear measuring instrument or other optical measuring instruments. Al-Tubi (Ref. 21) investigated the impact of tooth flank roughness and lubricant film thickness on the micropitting initiation process for different load stages. To evaluate the micropitting progress, the tooth flank surface quality was captured after each load stage using a microscope; the tooth profile deviations were captured after the last load stage using a CNC gear measuring instrument. Further, Al-Tubi calculated the specific lubricant film thickness for different points on the tooth flank, based on analytical models. Comparing the experimental results and analytical calculations, Al-Tubi discovered that the initiation of the micropitting starts to occur in the tooth root area, where the maximum contact stress leads to a minimum of lubricant film thickness. Moorthy (Ref. 22) studied gears with varying coatings and their influence on the initiation of micropitting damage. Contact fatigue tests have been carried out and the tested gear tooth flank surfaces were analyzed using a scanning electron microscope and compared to untested gears. Moorthy determined that micropitting is primarily initiated by sharp valleys on the tooth surface, when the valleys are preferentially orientated against the tooth sliding direction.

Most of the published research work uses offline-capable, optical measurands to quantify the natural provoked pitting

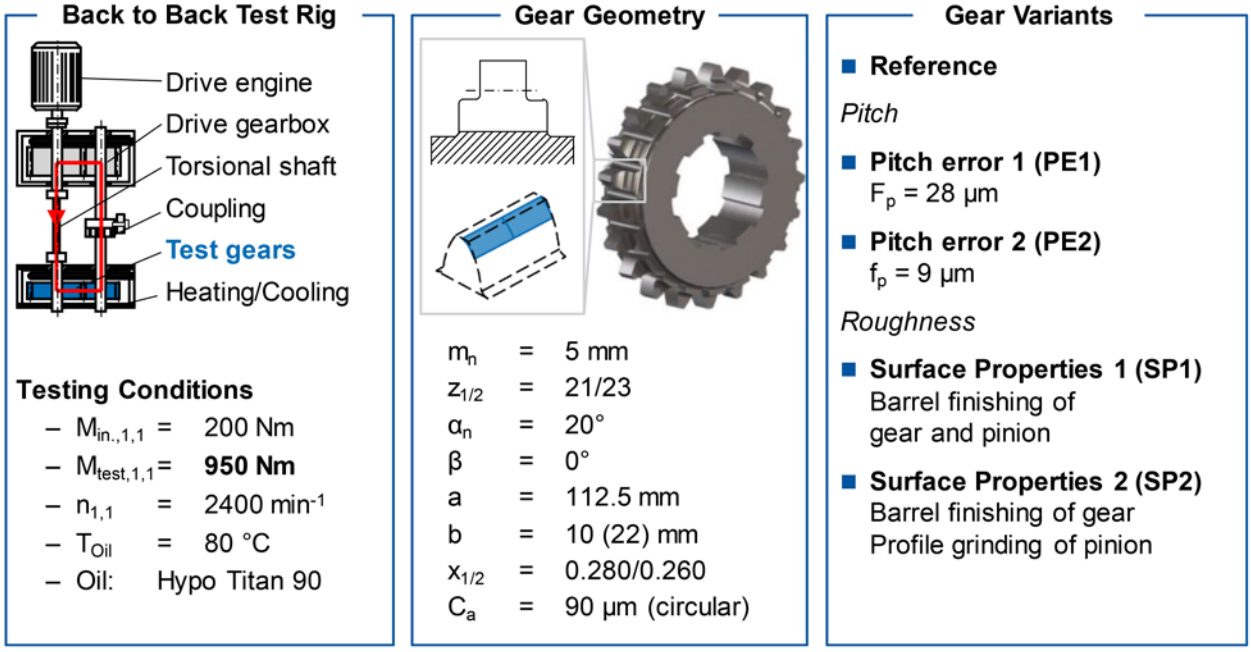

Figure 3 Conception of the study.

degradation of gears — or the pitting degradation is induced artificially. So far, there are rarely publications that use acceleration or AE sensors to monitor the pitting damage progression during load capacity tests. Whereas, the investigation in this paper presents online-capable geartrain monitoring methods using acceleration and AE sensors that allow detection of pitting damages during gear operation.

Experimental Design

In this section the experimental setup will be described. The back-to-back (B2B) test rig and the applied gears are explained, as well as the sensor setup used to acquire the data. Furthermore, the theory of the applied feature extraction methods is also discussed.

Conception of the Study

The pitting load-carrying capacity tests in this report are carried out on a B2B gear test rig with a center distance of $a = 112.5$ mm. The principle of the B2B gear test rig is standardized according to DIN ISO 14635 (Ref. 23). The test rig consists of a power circle, which consists in particular of the test gears, a drive gearbox, a torsional shaft and a coupling (Fig. 3).

After running-in at a torque of $M_{in.,1.1} = 200$ Nm, all tests were run at a test load of $M_{test,1.1} = 950$ Nm in order to enable a classification of the test variants on a constant load level. The gear speed is $n = 2{,}400\ min^{-1}$ for the entire test run. The test temperature is regulated to $T_{Oil} = 80°C$ with sump lubrication; Hypo Titan 90 oil is used as lubricant. The gear geometry is an established test geometry of type 21/23 with an involute tooth form, using a stepped tooth root according to Tobie with a common tooth width of $b = 10$ mm for a secure separation of pitting and tooth root safety regarding the investigation (Ref. 24). In addition to a crowning on the pinion of $C_{\beta,pinion} = 2$ µm and $C_{\beta,gear} = 1$ µm on the gear to avoid edge loading, a circular tip relief of $C_a = 90$ µm is used for the two gears to avoid premature tooth engagement.

Five different variants were investigated depending on their geometry and final manufacturing step. To classify the test results, a reference variant was first tested, which was manufactured without any deviations. The other four variants differ in geometric pitch errors and tooth flank roughness. The "Pitch Error 1" (PE1) variant is characterized by a cumulative pitch error of $F_p = 29$ µm compared to the reference, whereby the "Pitch Error 2" (PE2) variant has a single pitch error of $f_p = 9$ µm. The two variants — "Surface Properties 1 and 2" — differ in terms of surface characteristics and their final manufacturing step. For the "Surface Properties 1" (SP1) variant, both gear and pinion were barrel-finished to minimize tooth flank roughness. In the "Surface Properties 2" (SP2) gearset, only the gear is barrel-finished. In the B2B test rig the gear is paired with a profile ground pinion. The different gear qualities allow testing significant differences of selected gear properties to demonstrate the robust pitting detection method. For the load capacity tests, all test variants were made from case hardened steel (DIN EN 10084).

Measured Gears

Figure 4 shows the measurement results of the gear geometry deviations and the roughness. According to the measurement results, there is a clear difference between the individual variants. With a total pitch deviation of $F_P = 29.3$ µm for the PE1 variant, and a single pitch deviation of $f_p = 9.5$ µm for the PE2 variant, the given specifications were reached. The variants SP1 and SP2 also show a lower roughness compared to the reference. This allows differences or similarities in pitting detection to be traced back to the deviations.

Sensor Instrumentation

The instrumentation in Figure 5 was applied on the B2B gear test rig. Two identical piezoelectric accelerometers (Kistler, Type 8702) were placed on the bearing shell, mounted orthogonally and oriented to measure radial acceleration components. This sensor application aims for measuring radial accelerations resulting from locally distributed pitting. The accelerometer signals were acquired with a sampling frequency of 200 kHz. (*For the acceleration sensor signals the data acquisition board PXIe-4464 from National Instruments with an ADC resolution of 24 bits was used.*) Additionally, one AE sensor, provided as piezo-ceramic sensor, was applied on the bearing shell of the

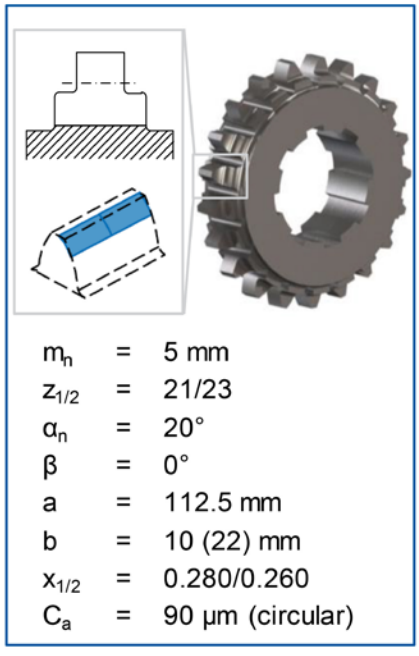

	V#	Variant	$f_{p,max}$ / µm	Q	F_p / µm	Q	$R_{a,av.,3\ teeth}$ / µm
Gear - z=23	V1	Reference	3.0	Q3	3.0	Q1	0.26
	V2	Pitch error 1	1.5	Q1	7.9	Q2	0.26
	V3	Pitch error 2	1.7	Q2	7.7	Q2	0.24
	V4	Surface Properties 1	4.4	Q5	16.1	Q4	**0.05**
	V5	Surface Properties 2	2.4	Q3	15.9	Q4	**0.13**

Key

- F_p — Cumulative pitch error
- $f_{p,max}$ — Maximal single pitch error
- $R_{a,av.,3\ teeth}$ — Average roughness over three tooth flanks
- Q — Toothing quality (DIN 3962-1)

Figure 4 Measured pitch error and roughness.

test gears ±45° to the acceleration sensors. Because it is assumed that the pitting initiation process begins with high frequency AE impulses above 50 kHz, an AE sensor with a bandwidth of 150 kHz was selected and sampled with 500 kHz. (*For the AE sensor signals the data acquisition board PXIe-6341 from National Instruments with an ADC resolution of 16 bits was used.*) The oil temperature within the test gearbox housing was measured using a Pt1000 thermocouple and acquired with a sampling frequency of 1 kHz. The angular information of the driven shaft is also used in this paper for resampling methods to describe the vibration signals in angular-domain. Therefore, the instantaneous shaft rotation angle of the torsional shaft was acquired using an incremental magnetic encoder with a rotation angle resolution of 15 bits.

The data of all sensors were recorded synchronously every 10 minutes with duration of 10 seconds using a multi-channel measurement system. The start of a measurement procedure was triggered by the incremental encoder at a defined rotation angle of the pinion. (*To ensure a synchronous sampling of all measurement channels a custom-build measurement application was developed in LabVIEW to trigger the data acquisition of digital encoder signals and analog vibration and temperature signals for a defined torsional shaft rotation angle point.*)

Pitting Diagnosis System

The data were processed to extract quantifiable indicators for the pitting damage. The angular signal resampling, the feature extraction, feature evaluation and feature selection constitute the proposed pitting diagnosis system (Fig. 6).

Pre-processing. Before the feature extraction step, the measurement signals data have to be pre-processed. First the instantaneous shaft angle is extracted from the incremental encoder signal. This is then used for resampling (Ref. 25) the acceleration sensor and AE sensor data into angle-dependent signals. This data format allows a speed-independent vibration signal processing using the order spectrum, and smearing of the vibration signals in the spectral representation, due to speed variations, is reduced. This enables the extraction of more robust features for the failure detection. Additionally, the logged run times and load cycles of the load capacity tests are pre-processed and merged to make them available for subsequent signal processing stages.

Feature extraction. Afterwards sensor-customized features will be extracted from the acquired sensor data. The following feature extraction methods were realized in this paper. To evaluate the impact of tooth flank pitting on the oil temperature the four central moments mean value, variance, skewness and kurtosis of the distributions from the sampled temperature data were calculated, whereas kurtosis w is defined as:

$$w = \frac{1}{N}\sum_{k=1}^{N}\left(\frac{x_k-\mu}{\sigma}\right)^4 \tag{1}$$

And the standard deviation σ and mean value μ are defined as:

$$\sigma = \sqrt{\frac{1}{N}\sum_{k=1}^{N}(x_k-\mu)^2}, \qquad \mu = \frac{1}{N}\sum_{k=1}^{N}x_k. \tag{2}$$

Additionally, the root mean square (RMS) value was used as a feature. From the accelerometer and AE sensor signals the same features are generated as for the oil temperature sensor. Locally distributed tooth pitting failures stimulate additional vibrations with the order of one shaft revolution and their harmonics. This causes amplitude modulation effects and sidebands in the order spectrum. The goal is to map these effects into additional features, which are generated by calculating the spectral power density for 9 defined frequency intervals. The frequency intervals range from the i^{th} harmonic of the gear mesh order to the i+1 harmonic, respectively, excluding the harmonics itself. Other significant features are extracted using the continuous

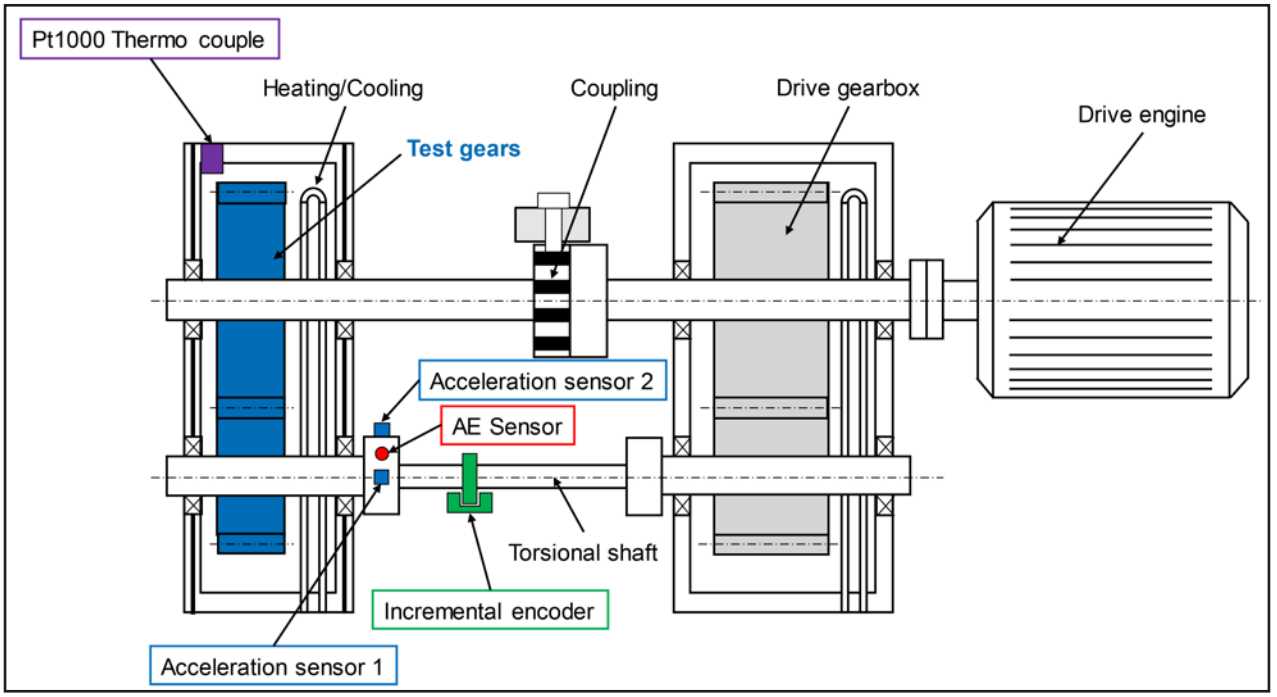

Figure 5 Sensor instrumentation for the B2B gear test rig.

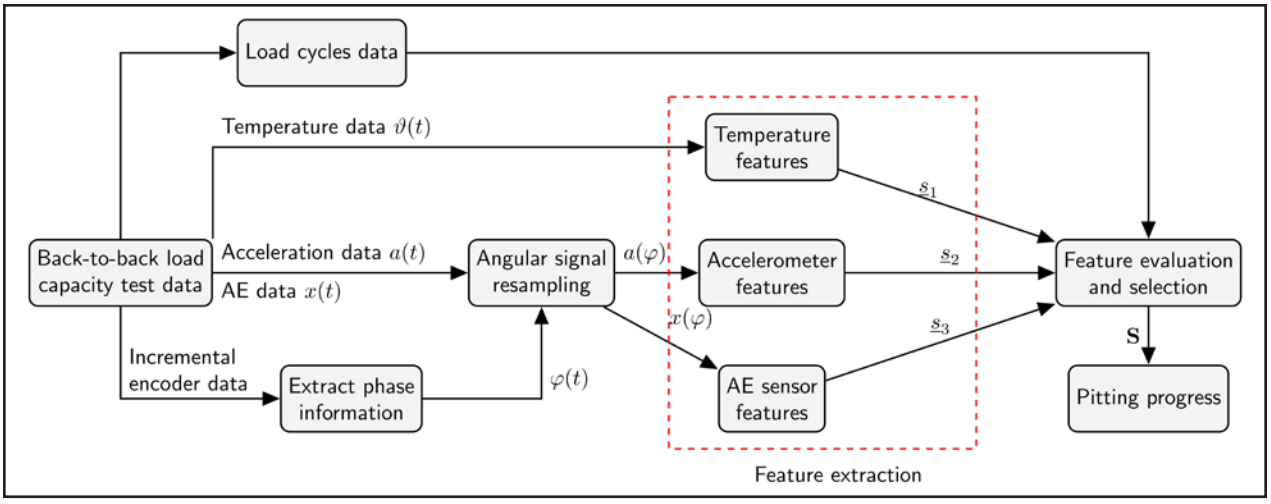

Figure 6 Schematic diagram of the proposed pitting diagnosis system.

wavelet transform (CWT):

$$X\omega(a,b) = \frac{1}{\sqrt{|a|}} \int_{-\infty}^{\infty} x(t) \cdot \Psi\left(\frac{t-b}{a}\right) dt \quad (3)$$

In the CWT the analyzing function is not a single variable. Analogous to ω in the Fourier transform, in the CWT wavelets are compressed or stretched using variable *a*. Therefore, executing the CWT on a signal using high-scaled wavelets leads to a low time resolution and high-frequency resolution, and vice versa for low scale factors (Ref. 29). In this paper the CWT coefficients were calculated using a Morlet wavelet. Afterwards the statistical values such as mean, variance and kurtosis from the CWT coefficients are generated to obtain CWT-based features. Because wavelets provide good localization at high frequencies and are sensitive to impulsive signals, they can be used for detecting local gear faults — like pitting. In addition to the already mentioned features, in this paper further features are generated from a bandpass filtered version of the AE sensor signals with a filter center frequency of 130 kHz. Here again statistical values are extracted to obtain features out from the bandpass filtered AE sensor signal. For one acquired measurement sample every 10 minutes, a set of one-dimensional features is generated. In case of M consecutive measurement samples, the feature extraction methods will generate M-dimensional feature vectors.

Feature evaluation. In the next signal processing step the generated features are being normalized to a uniform value range to allow a consistent feature evaluation. Although the measured sample data points were labeled using two classes (healthy gears and pitted gears), the problem is that the extracted feature values show an overlapping of the class distributions. Therefore, the Fisher discriminant criterion (Ref. 26) was used to find a class separation measure for every labeled feature vector. The Fisher criterion:

$$J_i = \frac{(\mu_2 - \mu_1)^2}{\sigma_1^2 + \sigma_2^2} \quad (4)$$

is defined as the ratio of the between-class variance to the within-class variance for a given feature *i*, whereby μ_j and σ_j^2 are the mean and variance, respectively, of the feature values of class *j*. In the last processing step those features with the highest separation value J_i are selected to depict the correlation between the pitting progress and the feature values. The assumption is that the selected features have the highest sensitivity with respect to pitting damage.

Results

This section presents the results generated by the applied feature extraction on the acceleration and AE sensors.

Testing results. Figure 7 shows the results of the load capacity tests. The upper part of the figure shows the damage patterns and the lower part shows the run times of the variants up to the point of damage. Except for the SP2 variant — which failed with a broken tooth over the stepped tooth root — all other variants failed from pitting. The results of the investigation show different running times for the gearset variants. However, since only one gearset-per-variant was tested, it is not possible to make a statistically reliable statement about the effects of roughness and pitch deviations on the tooth flank loading capacity.

Acquired sensor signals. The above-mentioned load capacity tests lead to the acquired signals in Figure 8 and Figure 9. As already in context with the signal processing chain in Figure 6 referenced, locally distributed tooth pitting induces additional vibrations. This is clear in the order spectra of acceleration sensor 1(Fig. 8). The left plot shows the order spectrum of gears without damage from the PE2 load capacity test. Here, acceleration amplitudes with the gear meshing order (GMO) and its harmonics are dominating the signal spectrum. The inset in the right order spectrum shows the pitting damage. Here, an extensive stimulation of sidebands at one order around the GMO's harmonics can be observed. This supports the idea of extracting features out of the sideband amplitudes between the GMO's harmonics.

In Figure 9 the Wigner-Ville distribution of the AE sensor signal from the PE2 test is shown. And again, the left plot represents the angle-order distribution of the AE signals without any gear damage, whereas the right plot shows the AE signal distribution of a pitted tooth flank in meshing contact. The figure shows that pitting leads to excitation of frequency components around 130 kHz. Therefore, the abovementioned statistical features, generated from the bandpass-filtered AE sensor signal, allow gathering additional robust pitting features.

Discussion of suitable features. After the sensor signals were processed using the signal processing chain in Figure 6, only the features with the highest Fisher criterion value will be presented in this discussion. For a clearer presentation, only a few features are shown in the following figures. The below discussed features are normalized through all tests to zero-mean feature values with a standard deviation of $\sigma = 1$ using translation and scaling.

Pitch error (PE) tests. In the gearset variants PE1 and PE2 (Fig. 10), the feature values generated from the oil temperature sensor did not identify any abnormalities. However, the kurtosis feature of the CWT coefficients generated from the AE sensor and the calculated spectral power densities between the 7th and 8th harmonic of the GMO, generated from the acceleration sensors, provided usable feature values. In the PE1 test it can be observed that the features show a significant value slope near the end of test run time.

In the PE2 test, the pitting could be detected 70 minutes (corresponds to 94% of test run time) before the complete pitting damage occurred. The indication is visible using both acceleration sensors and the AE sensor at a motor speed of 2,400 rpm. As shown in the right plot of Figure 10, first abnormalities in the feature values could be detected about 8 hours (corresponds to 68% of test run time) before complete pitting damage. Visual inspections were made, but quantifiable evidence of the pitting initiation requires non-intrusive measurements such as ultrasonic scans or X-ray measurements.

Surface properties (SP) tests. The evaluation of the features generated from the SP tests showed that in comparison to the PE tests the oil temperature within the tested gears increased with tooth pitting. The authors cannot explain how the gear geometry deviations influence the oil temperature. To answer this question further investigation is required. In Figure 11 the left plot shows the resulting features for the SP1 test, where pitting could be detected 230 minutes (corresponds to 91% of test

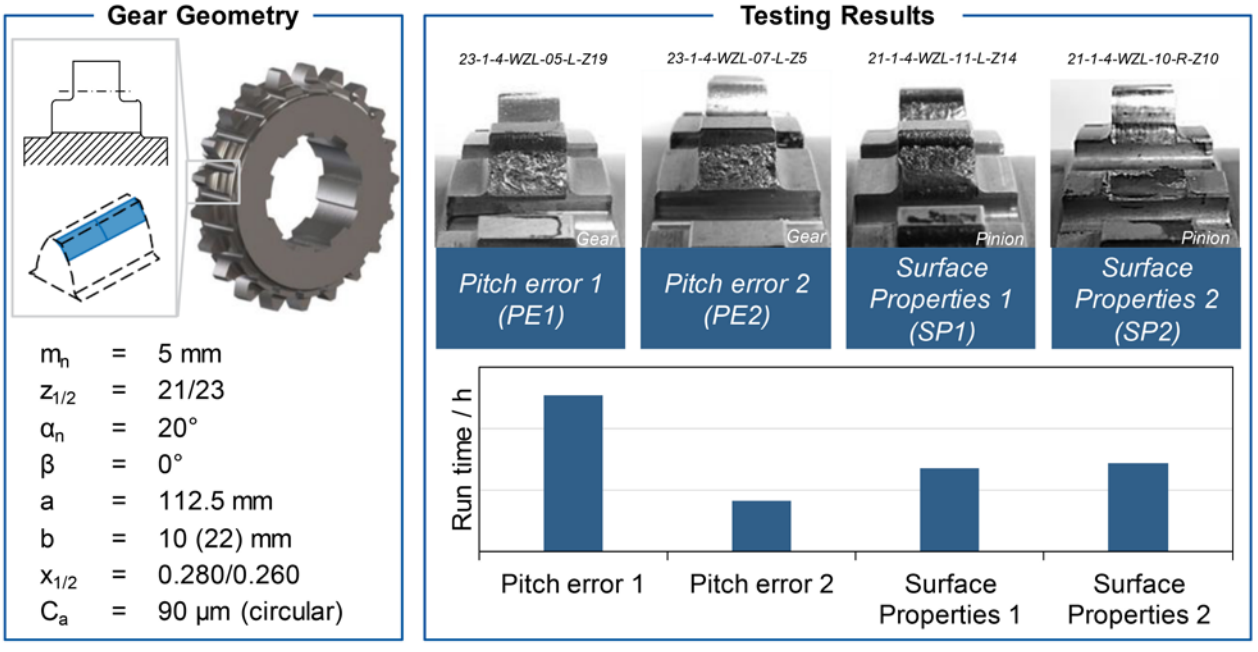

Figure 7 Testing results.

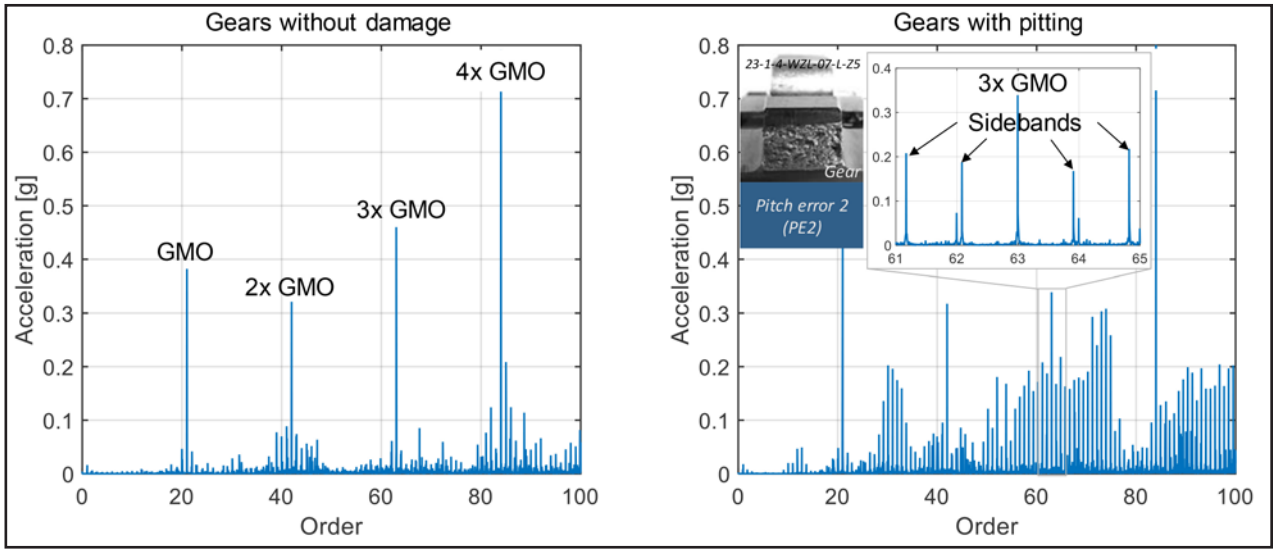

Figure 8 Order spectra of acceleration sensor 1 signal (PE2 test).

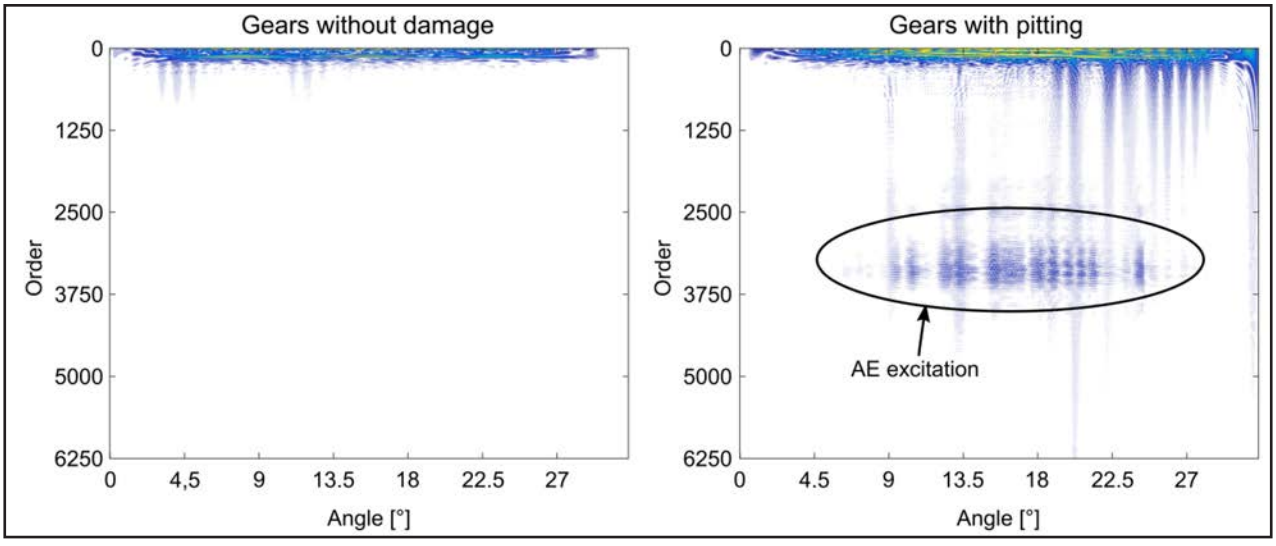

Figure 9 Wigner-Ville distribution of AE sensor signal (PE2 test).

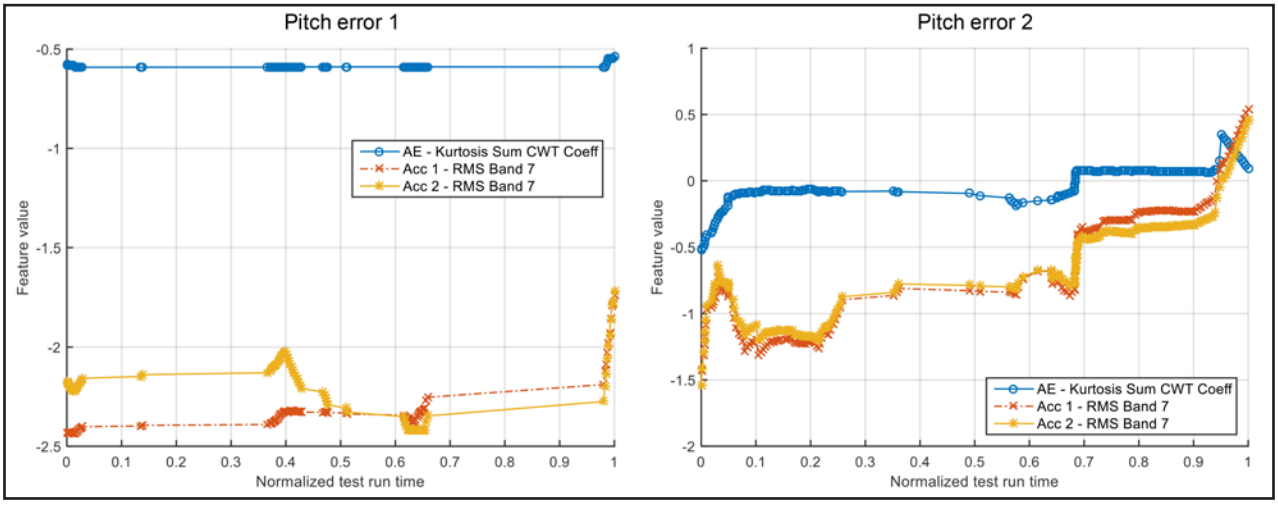

Figure 10 Pitting detection features generated from PE1 and PE2 tests.

run time) before complete pitting damage occurred at a motor speed of 2,400 rpm. In addition to already discussed features, in tests PE1 and PE2 additional features show pitting development.

Because the SP2 variant failed with a broken tooth over the stepped tooth root before any pitting occurred, no significant feature value variations are generated in this test, as shown in the right plot in Figure 11.

Comparison between acceleration and AE sensor. Both sensor techniques — acceleration and AE sensors — are suitable for the detection of pitting effects. This statement is valid with the premise that the used feature extraction methods are adjusted for the used sensor type, because of the different physical measurement variables and different sensor bandwidth.

Acceleration sensors showed a more sensitive behavior to pitting damage using features that concentrate on the evaluation of the sideband spectrum. AE sensors seem to be more sensitive to high-frequency elastic waves and, therefore, to impulse signals, which can be revealed using CWT coefficients. The use of AE sensors does not automatically ensure earlier pitting detection compared to accelerometers; it is possible that an AE sensor with greater bandwidth could provide earlier detection.

Nevertheless, the AE sensor has one important advantage compared to the accelerometer, i.e. — generating features from AE signals at a high-frequency range improves the distinction between different gear and test rig vibrations. The AE measures above the gear mesh frequency and its harmonics. Specific gear failure types can be identified, which can occur in different spectral ranges.

Conclusion

The experimental study showed that early detection of pitting damage is possible a few hours before severe pitting occurred on the tooth flanks. The results demonstrated the capability of accelerometers as well as acoustic emission (AE) sensors for indicating pitting damage on spur gears. Here, the automated evaluation of generated features using the Fisher criterion showed that, because of different measuring principles, the acceleration sensor and the AE sensor need sensor-specific feature extraction methods. Analyzing the sidebands of the acceleration sensor's order spectrum and calculating the statistical measurands of the AE sensor's wavelet coefficients provided the best results. This experimental study does not show that pitting is detectable with AE sensors earlier than with the use of acceleration sensors. Furthermore, recognize the influence of pitch

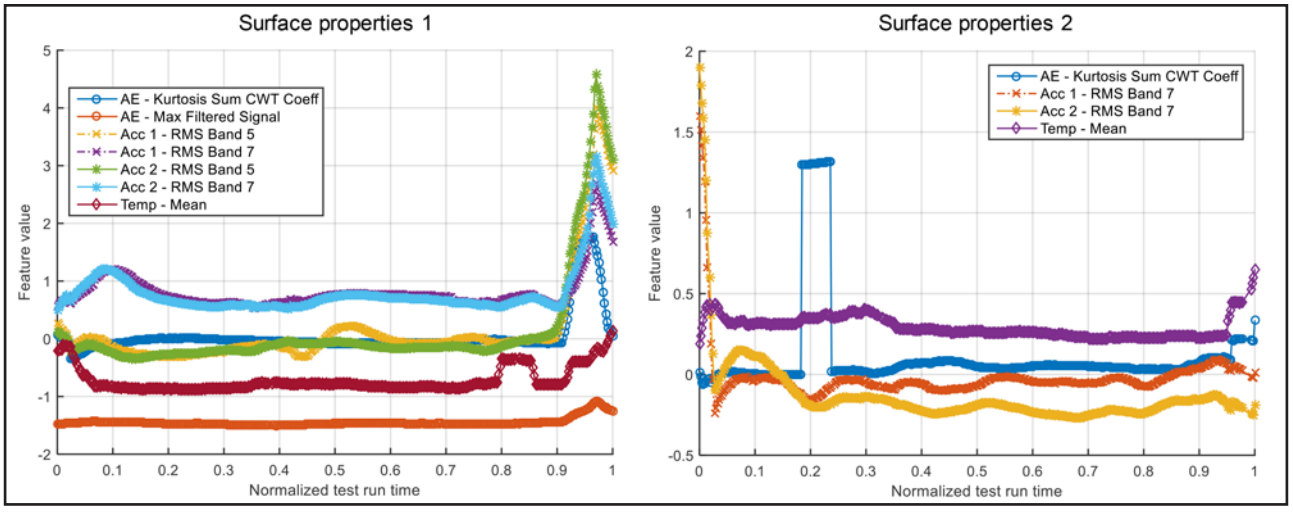

Figure 11 Pitting detection features generated from SP1 and SP2 tests.

deviations and different flank roughness. More load capacity tests with a larger sample size of gear variants must be carried out to allow statistically reliable propositions about the influence the manufacturing deviations have on gear life.

High-pitch deviations lead to a greater variation of the feature values than low, average flank roughness. Furthermore, more sensitive features to pitting damage are available if the flanks of the gear variant have a low- average roughness. Therefore, the assumption can be made that gears manufactured with a low-average flank roughness provide more robust pitting detection features; this also must be demonstrated with more testing. Sensitive features to pitting damage could be identified also for different pitch deviations. Overall, the investigations showed that the applied signal processing algorithms and features are tolerant of gear geometry deviations such as pitch deviations and tooth flank roughness.

Outlook

Based on the presented results, further measurements with a larger number of test gears must be performed to learn whether average tooth flank roughness has a greater impact than pitch error deviations on the pitting detection capability. Answering these questions could improve the future manufacturing process to guarantee, on the one hand, robust pitting detection methods and, on the other hand, a long service life without pitting damage. Additionally, the presented pitting detection methods also have to be verified with a greater sample size of tested gears. However, these gears should have comparable geometry deviations to control the main factors affecting pitting damage like geometry parameters and surface roughness. Furthermore, these signal processing methods may possibly be useful in evaluating gear quality such as at end-of-line testing of gearboxes.

Acknowledgment. *This work was supported by the Federal Ministry for Economic Affairs under the German National Aeronautical Program DeFiHog (20T1505). Thanks to Rolls-Royce Germany for permission to publish the results.*

References

1. Rolls-Royce (2017). "Rolls-Royce sets new aerospace record with UltraFan Power Gearbox," from *https://www.rolls-royce.com/media/our-stories/press-releases/2017/04-09-2017-rr-sets-new-aerospace-record-with-ultrafan-power-gearbox.aspx.*
2. National Aeronautics and Space Administration (2007): *NASA Systems Engineering Handbook,* CreateSpace Independent Publishing Platform.
3. Mohand, Slaoui-Hasnaoui, F., T. Tameghe and G. Ekemb. "Wind Turbine Condition Monitoring — State-of-the-Art Review: New Trends and Future Challenges," *Energies* 7 (4), S. 2595–2630. DOI: 10.3390/en7042595, 2014.
4. Mokhtari, N., M. Grzeszkowski and C. Guhmann. "Vibration Signal Analysis for the Lifetime Prediction and Failure Detection of Future Turbofan Components," *Technische Mechanik*; 37; 2–5; 422–431; ISSN 2199-9244 / 2,78 MB. DOI: 10.24352/UB.OVGU-2017-118, 2017.
5. Klocke, F. and C. Brecher. Zahnrad-und Getriebetechnik; Auslegung-Herstellung-Untersuchung- Simulation. München, Carl Hanser, 2017.
6. Gappisch, M. "Über die Grübchenbildung an Evolventen-Stirnradverzahnungen," RWTH Aachen University Diss. Aachen, 1962.
7. Brecher, C., C. Löpenhaus, F. Goergen and D. Mevissen. Erweiterte Schadensanalyse von Grübchenausbrüchen an einsatzgehärteten Zahnrädern. Forschung im Ingenieurwesen 81, 2017, 2–3, S. 221–232.
8. Santus, C., M. Beghini, I. Bartilotta and M. Facchini. "Surface and Subsurface Rolling Contact Fatigue Characteristic Depths and Proposal of Stress Indexes," *International Journal of Fatigue* 45 (2012), S. 71–81.
9. Neupert, B. Berechnung der Zahnkräfte Pressungen und Spannungen von Stirn-und Kegelradgetrieben, RWTH Aachen University Diss. Aachen, 1983.
10. Ding, Y. and J.A. Gear. "Spalling Depth Prediction Model," *Wear* 267, 2009, 5–8, S. 1181–1190.
11. Ding, Y. and N.F. Rieger. "Spalling Formation Mechanism for Gears," *Wear* 254, 2003, 12, S. 1307–1317.
12. ISO 6336 Teil 1; September 2006. Calculation of Load Capacity of Spur and Helical Gears — Basic Principles, Introduction and General Influence Factors.
13. AGMA 2001-D04; Dezember 2004. Fundamental Rating Factors and Calculation Methods for Involute Spur and Helical Gear Teeth.
14. Löpenhaus, C. "Untersuchung und Berechnung der Wälzfestigkeit im Scheiben-und Zahnflankenkontakt," RWTH Aachen University Diss. Aachen 2015.
15. Hertter, T. "Rechnerischer Festigkeitsnachweis der Ermüdungstragfähigkeit Vergüteter und Einsatzgehärteter Stirnräder," TU München Diss. München, 2003
16. Börnecke, K. Beanspruchungsgerechte Wärmebehandlung von Einsatzgehärteten Zylinderrädern, RWTH Aachen University Diss. Aachen, 1976.
17. Scheer, C. and W. Reimche and F.-W. Bach, 2007: "Early Fault Detection at Gear Units by Acoustic Emission and Wavelet Analysis," *Journal of Acoustic Emission* (Vol. 25).
18. Fernandes, P.J.L. and C. McDuling. "Surface Contact Fatigue Failures in Gears," *Engineering Failure Analysis* 4 (2), p. 99–107, 1997.
19. Cheng, Zhe; N. Hu, F. Gu, F. Fengshou and G. Qin. "Pitting Damage Levels Estimation for Planetary Gearsets Based on Model Simulation and Grey Relational Analysis," *Transactions of the Canadian Society for Mechanical Engineering*, Vol. 35, No. 3, 2011.

and Grey Relational Analysis," *Transactions of the Canadian Society for Mechanical Engineering*, Vol. 35, No. 3, 2011.
20. Tan, C. K., P. Irving and D. Mba. "A Comparative Experimental Study on the Diagnostic and Prognostic Capabilities of Acoustics Emission, Vibration and Spectrometric Oil Analysis for Spur Gears," *Mechanical Systems and Signal Processing* 21 (1), p. 208–233, 2007.
21. Al-Tubi, I. S., H. Long, J. Zhang and B. Shaw. "Experimental and Analytical Study of Gear Micropitting Initiation and Propagation Under Varying Loading Conditions," *Wear* 328–329, p. 8–16, 2015.
22. Moorthy, V. and B.A. Shaw. "An Observation on the Initiation of Micropitting Damage in As-Ground and Coated Gears During Contact Fatigue," *Wear* 297 (1-2), p. 878–884, 2013.
23. DIN ISO 14635 Teil 1; Mai 2006. Zahnräder. FZG-Prüfverfahren. FZG-Prüfverfahren A/8,3/90 zur Bestimmung der relativen Fresstragfähigkeit von Schmierölen.
24. Tobie, T. "Zur Grübchen-und Zahnfusstragfähigkeit Einsatzgehärteter Zahnräder," Einflüsse aus Einsatzhärtungstiefe, Wärmebehandlung und Fertigung bei unterschiedlicher Baugröße, TU München Diss. München, 2001
25. Villa, L. F., A. Reñones, J.R. Perán, and L. J. de Miguel. "Angular Resampling for Vibration Analysis in Wind Turbines Under Non-Linear Speed Fluctuation," *Mechanical Systems and Signal Processing* 25 (6), p. 2157–2168, 2011.
26. Bishop, C. M. *Pattern Recognition and Machine Learning*, Corr. at 8. print. New York, NY: Springer (Information Science and Statistics), 2009.
27. Elasha, F., C. Ruiz-Cárcel, D. Mba, G. Kiat, I. Nze and G. Yebra. "Pitting Detection in Worm Gearboxes with Vibration Analysis," *Engineering Failure Analysis* 42, p. 366–376, 2014.
28. DIN 3962 Teil1: August 1978. Toleranzen für Stirnradverzahnungen. Toleranzen für Abweichungen Einzelner Bestimmungsgrößen.
29. Randall, R. Bond. Vibration-Based Condition Monitoring, Industrial, Aerospace and Automotive Applications. 1. Aufl. s.l.: Wiley, 2011.
30. M. Grzeszkowski & C. Gühmann = Department of Energy and Automation Technology, TU Berlin
31. P. Scholzen & C. Löpenhaus = Laboratory of Machine Tools and Production Engineering, RWTH Aachen
32. S. Nowoisky & G. Kappmeyer = Rolls-Royce Deutschland Ltd & Co KG

For more information.
Questions or comments regarding this paper? Contact Mateusz Grzeszkowski — *mateusz.grzeszkowski@tu-berlin.de.*

Mateusz Grzeszkowski is currently a research assistant at the Chair of Electronic Measurement and Diagnostic Technology (MDT) at the TU Berlin, with the emphasis on pattern recognition methods for monitoring spur gears and planetary gears. He has bachelor and master degrees — both in electrical engineering. His experience in machine monitoring started at the Bundesanstalt für Materialforschung und -prüfung (BAM) during his master thesis in 2014, where he developed a diagnostic system for monitoring a rail wheelset axle using a non-destructive acoustic emission measurement technology. After graduating he began his research work in 2015 with the topic on diagnostic methods for monitoring planetary gears at the TU Berlin in cooperation with Rolls-Royce Deutschland.

Prof. Clemens Gühmann has been a professor at the TU Berlin since 2003, where he heads the Chair of Electronic Measurement and Diagnostic Technology. His research interests are data-based and physical-based modelling, diagnostics, remaining useful lifetime prediction and control of mechatronic systems, as well as measurement data processing. Previously, he worked seven years in the automotive industry at IAV GmbH in the development of automated transmissions.

Philipp Scholzen received his Bachelor of Science (2014) and Masters degree (2016) in Mechanical Engineering at RWTH Aachen University, specializing in automotive engineering. From 20111 to 2016, he was a student worker at WZL working on gear testing, and is today a WZL research assistant. As a current PhD candidate at WZL, Scholzen's research topic is the operational behavior of powder metallurgical gears — especially NVH behavior regarding gear mesh excitation, structure-borne noise transfer, and the resulting noise emission.

Dr. -Ing. Dipl. -Wirt. -Ing. Christoph Löpenhaus has since 2014 served as Chief Engineer in the Gear Department of WZL, RWTH Aachen / Laboratory of Machine Tools and Production Engineering (WZL), RWTH Aachen. He previously held positions there as (2011–2014) Team Leader, Group Gear Testing Gear Department Chair of Machine Tools Laboratory of Machine Tools and Production Engineering (WZL) RWTH Aachen; (2010–2011) Research Assistant, Group Gear Testing Gear Department Chair of Machine Tools Laboratory of Machine Tools and Production Engineering (WZL) RWTH Aachen: (2007–2009) as Student Researcher, Group Gear Design and Manufacturing Calculation Gear Department Chair of Machine Tools Laboratory of Machine Tools and Production Engineering (WZL) RWTH Aachen; and (2004–2009) as a student in Industrial Engineering RWTH Aachen.

Dr.-Ing. Sebastian Nowoisky received his diploma (Dipl.-Ing.) at the TU Berlin in 2008, studying electrical engineering with the specialization on measurement techniques. He has since 2014 worked at Rolls-Royce Deutschland Ltd & Co KG as System Architect on the Power Gearbox monitoring system. In 2016 he earned his PhD at the TU Berlin in the field of mechatronic parameter identification of gearboxes. He previously worked 5 years at the TU Berlin as researcher at the Chair of Electronic Measurement and Diagnostic Technology (MDT), focused in the field of automated car gearboxes. In his professional experience, since 2008 Nowoisky has worked as project engineer in the maintenance department at ThyssenKrupp Metal Forming.

Dr.-Ing. Gregor Kappmeyer is a Rolls-Royce Associate Engineering Fellow for machining, working on machining technologies for current and future aero-engine projects at Rolls-Royce. From 2010–2011 he held positions as Chief of Commodity Rotatives, and from 2006–2009 he was head of manufacturing engineering and technology at Rolls-Royce Deutschland, focusing on machining R&T projects. In 1999 he earned his doctorate in manufacturing engineering on ultrasonic-assisted honing at the TU Braunschweig (1990 – 1997), following positions as team leader of the precision machining group and as a researcher at the Institut für Werkzeugmaschinen und Fertigungstechnik (IWF) TU Braunschweig.